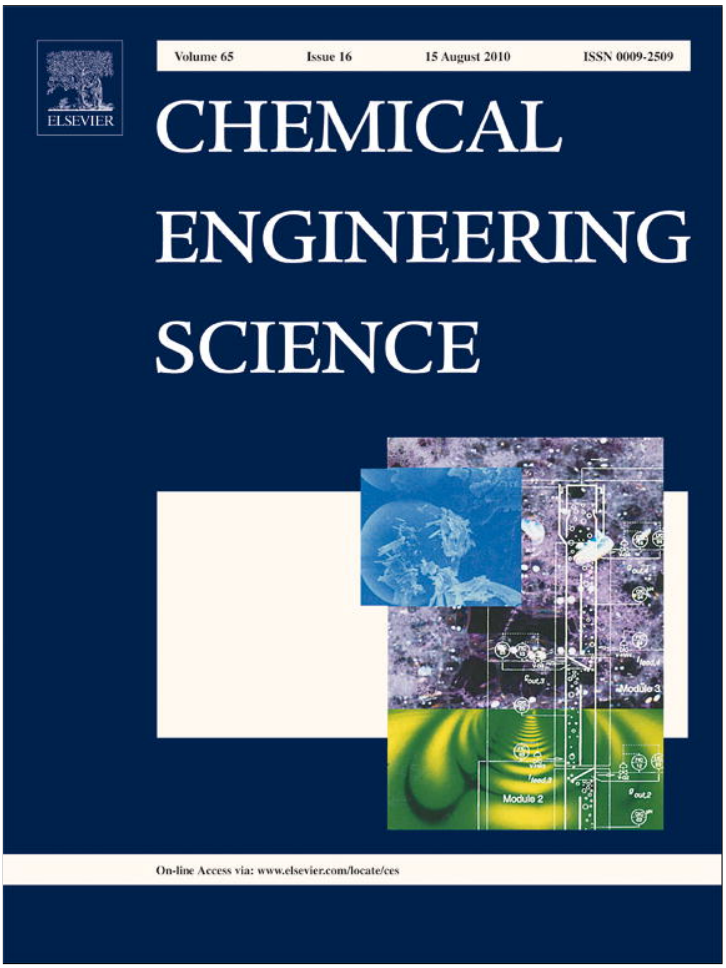

Chemical Engineering Science 65 (2010) 4720–4731

Contents lists available at ScienceDirect

Chemical Engineering Science

journal homepage: www.elsevier.com/locate/ces

# Predictive control of surface mean slope and roughness in a thin film deposition process

Xinyu Zhang [a], Gangshi Hu [a], Gerassimos Orkoulas [a], Panagiotis D. Christofides [a,b,*]

[a] Department of Chemical and Biomolecular Engineering, University of California, Los Angeles, CA 90095, USA
[b] Department of Electrical Engineering, University of California, Los Angeles, CA 90095, USA

ARTICLE INFO

*Article history:*
Received 17 February 2010
Received in revised form
13 May 2010
Accepted 14 May 2010
Available online 26 May 2010

*Keywords:*
Thin film growth
Process control
Film light reflectance
Computation
Dynamic simulation
Films

ABSTRACT

This work focuses on the development of a model predictive control algorithm to simultaneously regulate the surface slope and roughness of a thin film growth process to optimize thin film light reflectance and transmittance. Specifically, a thin film deposition process modeled on a one-dimensional triangular lattice that involves two microscopic processes: an adsorption process and a migration process, is considered. Kinetic Monte Carlo (kMC) methods are used to simulate the thin film deposition process. To characterize the surface morphology and to evaluate the light trapping efficiency of the thin film, surface roughness and surface slope are introduced as the root mean squares of the surface height profile and surface slope profile. An Edwards–Wilkinson (EW)-type equation is used to describe the dynamics of the surface height profile and predict the evolution of the root-mean-square (RMS) roughness and RMS slope. A model predictive control algorithm is then developed on the basis of the EW equation model to regulate the RMS slope and the RMS roughness at desired levels by optimizing the substrate temperature at each sampling time. The model parameters of the EW equation are estimated from simulation data through least-square methods. Closed-loop simulation results demonstrate the effectiveness of the proposed model predictive control algorithm in successfully regulating the RMS slope and the RMS roughness at desired levels that optimize thin film light reflectance and transmittance.



## 1. Introduction

Photovoltaic (solar) cells are an important source of sustainable energy. Currently, the limited conversion efficiency of the solar power prevents the wide application of solar cells. Thin-film silicon solar cells are currently the most developed and widely used solar cells. Research on optical and electrical modeling of thin-film silicon solar cells indicates that the scattering properties of the thin film interfaces are directly related to the light trapping process and the efficiencies of thin-film silicon solar cells (Krč et al., 2003; Müller et al., 2004). Recent studies on enhancing thin-film solar cell performance (Zeman and Vanswaaij, 2000; Poruba and Fejfar, 2000; Müller et al., 2004; Springer and Poruba, 2004; Rowlands et al., 2004) have shown that film surface and interface morphology, characterized by root-mean-square roughness (RMS roughness, $r$) and root-mean-square slope (RMS slope, $m$), play an important role in enhancing absorption of the incident light by the semiconductor layers. Specifically, significant increase of conversion efficiency by introducing appropriately rough interfaces has been reported in several works (Tao and Zeman, 1994; Leblanc and Perrin, 1994; Krč and Zeman, 2002). To provide a concrete example of this issue, we focus on a typical p-i-n thin-film solar cell (Fig. 1). In this thin-film solar cell, light comes into the hydrogenated amorphous silicon (a-Si:H) semiconductor layers (p, i, n layers) through a front transparent conducting oxide (TCO) layer (made, for example, of ZnO:Al), and part of this light is absorbed by the semiconductor layers before it reaches the back TCO layer. At the back TCO layer, the remaining light is either reflected back to the semiconductor layers to potentially be absorbed again or leaves the system by transmitting through the back TCO layer. The reflected light that is not absorbed reaches the front TCO layer again and this process of reflection and transmission is repeated until all the light leaves the cell or is absorbed by the cell. We focus on a thin film a-Si:H p-i-n solar cell with glass/ZnO:Al as the front TCO layer and ZnO:Al as the back TCO layer to demonstrate quantitatively the influence of surface/interface $r$ and $m$ on thin film light reflectance and transmittance.

Light scattering (Rayleigh scattering) occurs when the incident light goes through a rough interface (e.g., the front TCO surface or the TCO-p interface) where it is divided into four components: specular reflection, specular transmission, diffused reflection and diffused transmission; see Fig. 2 (Tao and Zeman, 1994; Leblanc

* Corresponding author at: Department of Chemical and Biomolecular Engineering, University of California, Los Angeles, CA 90095, USA. Tel.: +1 310 794 1015; fax: +1 310 206 4107.
*E-mail address:* pdc@seas.ucla.edu (P.D. Christofides).

0009-2509/$ - see front matter © 2010 Elsevier Ltd. All rights reserved.
doi:10.1016/j.ces.2010.05.025

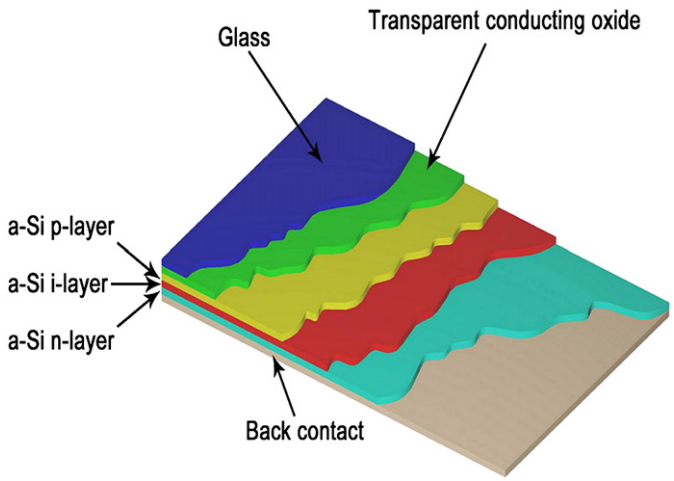


**Fig. 1.** Typical structure of a p-i-n thin-film solar cell with front transparent conducting oxide (TCO) layer and back contact.

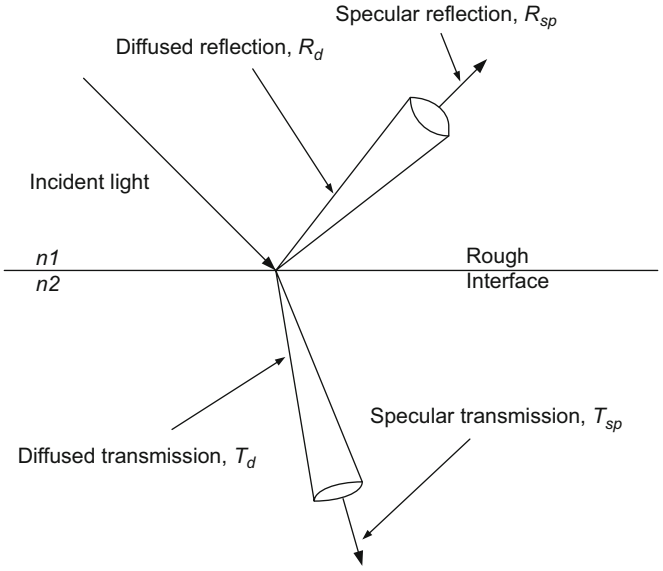


**Fig. 2.** Light scattering at a rough interface: specular reflection, $R_{sp}$, diffused reflection, $R_d$, specular transmission, $T_{sp}$, and diffused transmission, $T_d$. $n_1$ and $n_2$ are the refractive indices of the two substances above and below the rough interface, respectively.

and Perrin, 1994). If a rough thin film surface is illuminated with a beam of monochromatic light at normal incidence, the total reflectance, $R$, can be approximately calculated as follows (Davies, 1954):

$$R = R_0 \exp\left[-\frac{4\pi r^2}{\lambda^2}\right] + R_0 \int_0^{\pi/2} 2\pi^4 \left(\frac{a}{\lambda}\right)^2 \left(\frac{r}{\lambda}\right)^2 (\cos\theta + 1)^4 \sin\theta \exp\left[-\frac{(\pi a \sin\theta)^2}{\lambda^2}\right] d\theta, \quad (1)$$

where $R_0$ is the reflectance of a perfectly smooth surface of the same material, $r$ is the RMS roughness, $\theta$ is the incident angle, $\lambda$ is the light wavelength and $a$ is the auto-covariance length. It can be proved that $a = \sqrt{2}r/m$, where $m$ is the RMS slope of the profile of the surface (Bennett and Porteus, 1961). The numerical integration result of Eq. (1) is shown in Fig. 3. From this plot, it can be inferred that both $r$ and $m$ strongly influence the

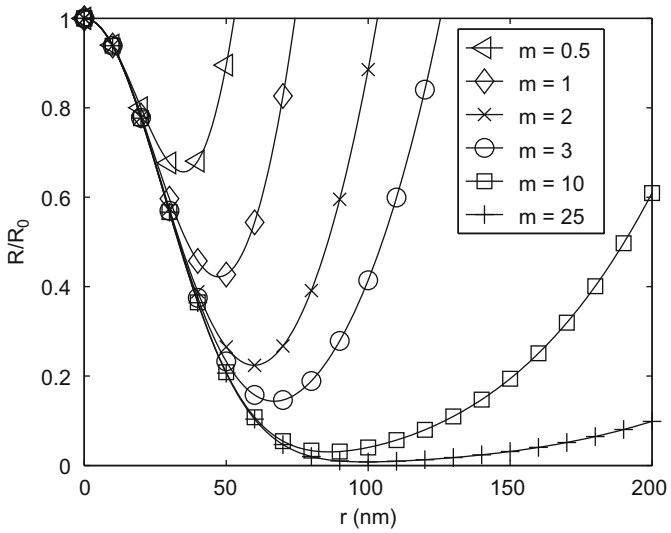


**Fig. 3.** Reflectance of thin film surface as a function of $r$ for different $m$.

intensity of light reflection (and therefore, light transmission) by the surface/interface. Specifically, in a thin-film solar cell, the objective is to maximize the generation of electricity in the i-layer, so it is necessary to control the intensities and directions of light reflection and transmission at the front and back TCO layers, as well as at the TCO-p and n-TCO interfaces by attaining proper values of $r$ and $m$ during the thin-film manufacturing process. Specifically, when light first comes into the front TCO layer, appropriate values of $r$ and $m$ are needed for the surface of the TCO layer to maximize the transmission, $T$, through the TCO layer. At the back n-TCO interface layer, certain surface morphology is also required to maximize the reflection, $R$, of light back to the cell. The distributions of the four components of light reflectance and transmittance are also affected by $m$ and $r$ (Krč and Zeman, 2002, 2004) even though this dependence cannot be expressed by an approximate equation like the one of Eq. (1). Therefore, it is important during the manufacturing of thin-film solar cells to regulate process input variables like precursor flow rates and temperature such that the surfaces/interfaces of the produced thin-film solar cells have appropriate values (set-points) of $r$ and $m$ that optimize light reflectance and transmittance.

In the context of modeling and control of thin film microstructure and surface morphology, two mathematical modeling approaches have been developed and widely used: kinetic Monte Carlo (kMC) methods and stochastic differential equation (SDE) models. KMC methods were initially introduced to simulate thin film microscopic processes based on the microscopic rules and the thermodynamic and kinetic parameters obtained from experiments and molecular dynamics simulations (Levine et al., 1998; Zhang et al., 2004; Levine and Clancy, 2000; Christofides et al., 2008). Since kMC models are not available in closed form, they cannot be readily used for feedback control design and system-level analysis. On the other hand, SDE models can be derived from the corresponding master equation of the microscopic process and/or identified from process data (Christofides et al., 2008; Ni and Christofides, 2005; Hu et al., 2009b–d). The closed form of SDE models enables their use as the basis for the design of feedback controllers which can regulate thin film surface roughness, film porosity, and film thickness using either deposition rate or substrate temperature as manipulated input (Hu et al., 2009b–d). Recent research work has also focused on multiscale modeling and identification methods for control of surface morphology (Varshney and Armaou, 2006). Furthermore, computationally

efficient multiobjective optimization methods for microscopic systems using *in situ* adaptive tabulation techniques have been developed (Varshney and Armaou, 2005, 2008). However, simultaneous feedback control of RMS slope and roughness of surface height profiles in thin film deposition processes has not been studied.

Motivated by the above considerations, this work focuses on the development of a model predictive control algorithm to simultaneously regulate the surface slope and roughness of a thin film growth process to optimize thin film light reflectance and transmittance. Specifically, a thin film deposition process modeled on a one-dimensional triangular lattice that involves two microscopic processes: an adsorption process and a migration process, is considered. Kinetic Monte Carlo methods are used to simulate the thin film deposition process. To characterize the surface morphology and to evaluate the light trapping efficiency of the thin film, surface roughness and surface slope are introduced as the root mean squares of the surface height profile and surface slope profile. An Edwards–Wilkinson (EW)-type equation is used to describe the dynamics of the surface height profile and predict the evolution of the RMS roughness and RMS slope. A model predictive control algorithm is then developed on the basis of the EW equation model to regulate the RMS slope and the RMS roughness at desired levels by optimizing the substrate temperature at each sampling time. The model parameters of the EW equation are estimated from simulation data through least-square methods. Closed-loop simulation results are presented to demonstrate the effectiveness of the proposed model predictive control algorithm in successfully regulating the RMS slope and the RMS roughness at desired levels that optimize thin film light reflectance and transmittance.

## 2. Thin film deposition process

In this section, a thin film growth process is considered and modeled by using an on-lattice kMC model on a triangular lattice. Vacancies and overhangs are allowed to develop inside the film (Hu et al., 2009a, d). Definitions of surface height profile, root-mean-square roughness, and RMS slope are also introduced in this section.

### 2.1. On-lattice kinetic Monte Carlo model

The one-dimensional triangular lattice in which the thin film deposition process takes place is shown in Fig. 4. Film growth occurs in the direction perpendicular to the lateral direction, i.e., the vertical direction as shown in Fig. 4. Periodic boundary conditions are applied in the lateral direction, i.e., the horizontal direction as shown in Fig. 4. In the triangular lattice, the maximum number of nearest neighboring particles around a given particle is six. In the one-dimensional triangular lattice model, a particle with only one nearest neighbor (and the rest five neighboring sites being vacant) is considered unstable and is subject to instantaneous surface relaxation. When a particle is subject to instantaneous surface relaxation, it moves to the nearest vacant site that is the most stable, i.e., the site with the most nearest neighbors; see Huang et al. (in press) for a detailed description of the relaxation process. To initiate the thin film deposition process, a fully packed and fixed substrate layer is placed in the bottom of the lattice at the beginning of the deposition process; see Fig. 4.

In this thin film deposition process, two different micro-processes take place and significantly influence the thin film surface morphology (Wang and Clancy, 2001; Yang et al., 1997): an adsorption process, where vertically incident particles are deposited from the gas phase into the thin film, and a migration process, where particles on the thin film overcome the energy barriers of their sites and move to neighboring vacant sites. In an adsorption process, the initial positions of the incident particles are randomly determined with a uniform probability distribution function in the gas phase domain. In a migration process, the probability that an on-film particle is subject to migration (i.e., migration rate) follows an Arrhenius-type law, where the pre-exponential factor and the activation energy are taken from a silicon film (Hu et al., 2009a). However, substrate particles and the particles fully surrounded by six nearest neighbors cannot move.

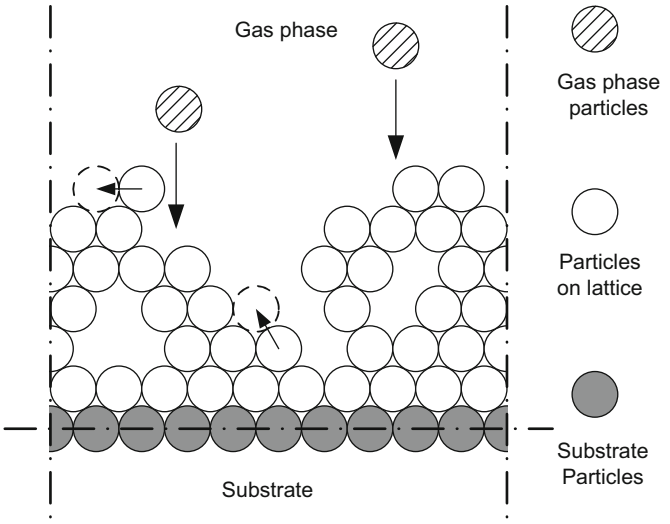


**Fig. 4.** Thin film growth process on a triangular lattice. The arrows denote adsorption and migration processes.

The stochastic nature of the microscopic deposition process is captured by using a kinetic Monte Carlo (kMC) algorithm to simulate the evolution of the deposition process. The microscopic rules of these micro-processes are used in the kMC algorithm to simulate the thin film deposition process. In the kMC simulation, each Monte Carlo event represents a specific microprocess, e.g., adsorption of a particle from the gas phase or migration of a particle on the thin film. In the kMC simulation, the time increment after a successfully executed Monte Carlo event depends on the total rate of all possible events in the lattice model of the thin film at the time of the execution of the event. In this work, a continuous-time Monte Carlo (CTMC)-type method (e.g., Vlachos et al., 1993) is used to implement the kMC simulations.

The thin film surface morphology depends on the adsorption and the migration processes. As a result of the complex interplay between the adsorption process and the migration process, the thin film surface morphology achieves a thermal balance. This thermal balance can be represented by certain values of surface roughness and surface slope, the definitions of which are introduced in the next subsection. The macroscopic variables of the deposition process have a strong influence on the resulting film surface morphology. The two variables that are considered in this work are the adsorption rate and the substrate temperature. Specifically, the adsorption rate, which is denoted by $W$, is defined as the number of deposited layers per second. The substrate temperature, which is denoted by $T$, influences the migration rate via the Arrhenius rate law.

We note that the deposition rate as an operating condition in this work is different from the rate of change of film thickness. The deposition rate here refers to the number of fully packed

layers deposited per second and, in a vapor deposition process model, is determined from the flux rate at the gas-phase/surface boundary. With a constant deposition rate, the same amount of particles is deposited in the same time period (in the sense of expected value). Meanwhile, with different substrate temperatures, different film microstructures may form with different film porosity and film thickness. Thus, process operating conditions like the deposition rate or the substrate temperature, can be constant or vary with respect to time. These operating variables can be used as the manipulated variables for the control of the thin film surface morphology expressed in terms of RMS surface slope and RMS surface roughness.

### 2.2. Definition of variables

In this section, two variables, RMS surface roughness and RMS surface slope, are precisely defined to characterize the film surface morphology and calculate the reflectance of a surface/interface. The surface height profile is used to represent the film surface morphology in the one-dimensional lattice model and is defined as the connection of the centers of the surface particles. Surface particles are the particles that can be reached from above in the vertical direction without being fully blocked by other particles on the film (Hu et al., 2009a, d). Fig. 5 shows an example of the surface height profile of a given thin film configuration. The RMS surface roughness and RMS surface slope can be then defined on the basis of the surface height profile of the thin film.

Surface roughness is a commonly used measure of thin film surface morphology. In this work, surface roughness is defined as the root mean square of the surface height profile. Specifically, the definition of RMS surface roughness is given as follows:

$$r=\left[\frac{1}{2L}\sum_{i=1}^{2L}(h_i-\bar{h})^2\right]^{1/2}, \tag{2}$$

where $r$ denotes the RMS surface roughness, $h_i$, $i=1,2,\ldots,2L$, is the surface height at the $i$-th position in the unit of layer, $L$ is the number of sites on the lateral direction, and $\bar{h}=(1/2L)\sum_{i=1}^{2L}h_i$ is the average surface height.

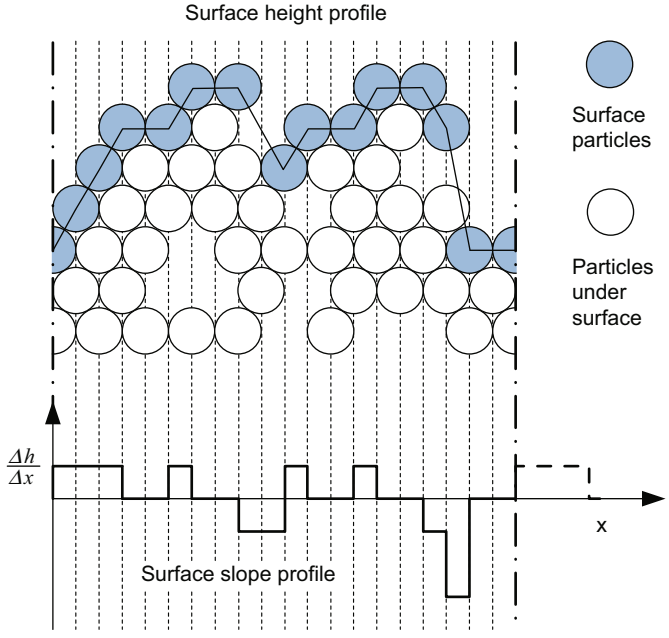


**Fig. 5.** An example showing the definition of the surface height profile and the calculation of the corresponding surface slope profile.

From the expression of surface light reflectance of Eq. (1) and the dependence of light reflectance in Fig. 3, the RMS surface slope is also an important variable that determines the surface morphology in addition to the RMS roughness. In this work, the RMS slope represents the extent of surface slope and is defined as the root-mean-square of surface slope profile similarly to the definition of the RMS roughness of Eq. (2) in the following form:

$$m=\left[\frac{1}{2L}\sum_{i=1}^{2L}(h_i^s)^2\right]^{1/2}, \tag{3}$$

where $m$ denotes the RMS slope and $h_i^s$, $i=1,2,\ldots,2L$, is the surface slope at the $i$-th position. Both $m$ and $h_i^s$ are dimensionless variables. The surface slope profile is obtained from the surface height profile using a first-order finite-difference approximation as follows:

$$h_i^s=\frac{(h_{i+1}-h_i)\sqrt{3}/2}{1/2}=\sqrt{3}(h_{i+1}-h_i), \tag{4}$$

where the constant, $\sqrt{3}$, is derived from the geometric ratio between the single-layer height and the interval between adjacent height positions in the triangular lattice. Due to the use of PBCs, the slope at the right most boundary position ($h_{2L}^s$) is computed from the right most and the left most surface heights, i.e., $h_{2L}^s=\sqrt{3}(h_1-h_{2L})$. Fig. 5 also shows an example of the surface slope profile obtained from the surface height profile.

The behavior of RMS slope, i.e., its dynamics and dependence on the operating conditions and on the lattice size, has been studied in previous work (Huang et al., in press). For the purpose of theoretical analysis and control design, the square of RMS roughness (surface roughness square, $r^2$) and the square of RMS slope (mean slope square, $m^2$), are used in the analysis and controller design later in this work. Specifically, the expected mean slope square increases from zero and reaches a steady state at large times. The dynamics and the steady-state values of the expected mean slope square depend on the operating conditions, i.e., the substrate temperature and the adsorption rate. Thus, the substrate temperature and/or the adsorption rate may be used as the manipulated inputs in the model predictive control design.

## 3. Closed-form dynamic model construction

### 3.1. Edward–Wilkinson model

The dynamics and evolution of the surface height profile of the thin film growth process of Fig. 4 can be described by an Edwards–Wilkinson (EW)-type equation (Edwards and Wilkinson, 1982; Family, 1986; Hu et al., 2009a; Huang et al., in press). The EW equation is a second-order stochastic PDE that has the following form (Edwards and Wilkinson, 1982; Hu et al., 2009a):

$$\frac{\partial h}{\partial t}=r_h+\nu\frac{\partial^2 h}{\partial x^2}+\xi(x,t), \tag{5}$$

subject to the following PBCs:

$$h(-L_0,t)=h(L_0,t),\quad \frac{\partial h}{\partial x}(-L_0,t)=\frac{\partial h}{\partial x}(L_0,t), \tag{6}$$

and the initial condition:

$$h(x,0)=h_0(x), \tag{7}$$

where $x\in[-L_0,L_0]$ is the spatial coordinate, $t$ is the time, and $r_h$ and $\nu$ are model parameters. Specifically, $r_h$ is related to the growth of average surface height and $\nu$ is related to the effect of surface particle relaxation and migration. Since $r_h$ is only related

to the average surface height, this term can be ignored for the purpose of modeling and control of the RMS slope, i.e., $r_h=0$, (Hu et al., 2009a; Huang et al., in press).

In the EW equation of Eq. (5), $\xi(x,t)$ is a Gaussian white noise term with the following expressions for its mean and covariance:

$$\langle \xi(x,t)\rangle = 0,$$

$$\langle \xi(x,t)\xi(x',t')\rangle = \sigma^2\delta(x-x')\delta(t-t'), \tag{8}$$

where $\langle\cdot\rangle$ denotes the mean value, $\sigma^2$ is a parameter which measures the noise intensity, and $\delta(\cdot)$ denotes the standard Dirac delta function.

To obtain the dynamics of the RMS slope, we first solve the EW equation using modal decomposition. A direct computation of the eigenvalue problem of the linear second-order operator of Eq. (5) yields the eigenvalues, $\lambda_n$, and the eigenfunctions, $\overline{\phi}_n(x)$. Due to the eigenspectrum of the second-order operator and the nature of the deposition process, $\lambda_0=0$ (which corresponds to the average surface height) and $\lambda_n<0$ for $n\geq 1$. The solution of Eq. (5) is then expanded in an infinite series in terms of the eigenfunctions. By substituting the expansion into Eq. (5) and taking the inner product with the adjoint eigenfunctions, the following system of infinite stochastic ordinary differential equations (ODEs) is obtained:

$$\frac{d\alpha_n}{dt} = \lambda_n\alpha_n + \xi_\alpha^n(t), \quad n=0,1,\ldots,\infty, \tag{9}$$

where $\xi_\alpha^n$ is the projection of the noise $\xi(x,t)$ in the $n$-th ODE. Since the infinite stochastic ODEs of Eq. (9) are linear and uncoupled, the state variance can be directly obtained from the analytical solution of Eq. (9) as follows:

$$\langle \alpha_n^2(t)\rangle = -\frac{\sigma^2}{2\lambda_n} + \left(\langle \alpha_n^2(t_0)\rangle + \frac{\sigma^2}{2\lambda_n}\right)e^{2\lambda_n(t-t_0)}, \quad n=1,2,\ldots,\infty. \tag{10}$$

The dynamics of the surface roughness square and of the mean slope square can be obtained from the solution of the state variance of Eq. (10). The surface roughness square in the continuum domain in which the EW equation is constructed is defined as the square of the standard deviation of the surface height profile from its average height as follows:

$$r^2(t) = \frac{1}{2L_0}\int_{-L_0}^{L_0}[h(x,t)-\overline{h}(t)]^2\,dx, \tag{11}$$

where $\overline{h}(t)=(1/2L_0)\int_{-L_0}^{L_0}h(x,t)\,dx$ is the average surface height which corresponds to the zeroth state in Eq. (9). The expected surface roughness square, $\langle r^2(t)\rangle$, can then be rewritten in terms of the state variance, $\langle \alpha_n^2(t)\rangle$, as follows:

$$\langle r^2(t)\rangle = \frac{1}{2L_0}\sum_{n=1}^{\infty}\langle \alpha_n^2(t)\rangle. \tag{12}$$

However, the mean slope square cannot be defined in the continuum domain similarly to the surface roughness square of Eq. (11) because such a definition leads to an infinite value of mean slope square (Huang et al., in press). To calculate the mean slope square and derive its dynamic behavior, the mean slope square should be obtained from the solution of the EW equation under a suitable finite-difference discretization of the continuum surface height profile. Specifically, a spatial discretization is introduced to the continuum domain, $[-L_0, L_0]$, with evenly distributed nodes in space. The number of nodes equals the lattice size of the kMC model, $L$. With the finite-dimensional discretization, the mean slope square of a discrete surface height profile can be computed in a similar fashion to Eq. (3) as follows:

$$m^2 = \frac{1}{2L}\sum_{i=1}^{2L}\left(\frac{h_{i+1}-h_i}{\Delta x}\right)^2, \tag{13}$$

where $h_i$ denotes the surface height at the $i$-th node and $\Delta x = L_0/L$ denotes the interval between two adjacent nodes. The expected mean slope square can then be expressed as the sum of weighted modal state variances as follows (Huang et al., in press):

$$\langle m^2(t)\rangle = \sum_{n=1}^{\infty}K_n\langle \alpha_n^2(t)\rangle \quad \text{where } K_n = \frac{2}{L(\Delta x)^3}\sin^2\left(\frac{n\pi}{2L}\right). \tag{14}$$

Using the analytical solutions of the expected surface roughness square of Eq. (12) and of the expected mean slope square of Eq. (14), we can obtain the behavior of the surface roughness square and of the mean slope square from the EW equation and from the lattice model. These analytical solutions will be later used to predict the evolution of the expected surface roughness square and of the expected mean slope square in the model parameter estimation and in the controller design.

**Remark 1.** The EW equation of Eq. (5) is appropriate as a dynamic model for a random deposition with instantaneous relaxation process, as was established in our previous research work (Hu et al., 2009a). Specifically, our previous work has focused on the scaling properties of the porous thin film deposition process used in this work and has rigorously demonstrated an EW-consistent behavior of this process. Thus, the EW equation is a good choice as the dynamic model for the evolution of surface height profile, especially from a control point of view. The applicability of the EW equation model for the control algorithm design is demonstrated via the numerical simulations in Section 5. In general, the EW equation is an appropriate model for many deposition processes with certain microscopic rules that lead to a thermal balance between adsorption and relaxation/migration during thin film growth.

**Remark 2.** The use of modal decomposition for order reduction of the EW equation of Eq. (5) is appropriate because the EW equation is linear in $h$ and its parameters are constant between two successive sampling times/control actions. Furthermore, the open- and closed-loop simulations in Section 5 demonstrate that the use of the modal decomposition to solve the model used for controller design yields very good closed-loop response.

### 3.2. Model parameter estimation and dependence on substrate temperature

In the EW equation of Eq. (5), there are three parameters $r_h$, $\nu$, and $\sigma^2$. The dependence of the model parameters, $\nu$ and $\sigma^2$, on the operating conditions, i.e., the adsorption rate and the substrate temperature, is determined from the kMC simulation data. In this work, we only consider the temperature dependence of model parameters and use the substrate temperature as the manipulated input for control purposes (see Section 4). Deposition rate is another choice for manipulated variable, and it can be implemented via the control of inlet flow rate and/or precursor concentration. Multivariable feedback control with temperature and deposition rate as manipulated variables can be done but it is outside the scope of this work.

In this work, the model parameter estimation is conducted on the basis of the RMS slope so that the dynamics of the surface slope can be captured by the EW equation in a more accurate fashion. Specifically, these parameters are estimated by matching the predicted evolution profiles of mean slope square to the ones obtained from the kMC simulations of the thin film deposition process in a least-square sense where the following cost is minimized:

$$\min_{\nu,\sigma^2}\sum_{k=1}^{N_1}\left[\langle m^2(t_k)\rangle - \sum_{n=1}^{\infty}K_n\langle \alpha_n^2(t_k)\rangle\right]^2, \tag{15}$$

where $N_1$ is the number of data points used for parameter estimation and $\langle m^2(t_k)\rangle$ is the expected mean slope square computed from

100 independent kMC simulations with identical and time-invariant operating conditions. The prediction of the state variance, $\langle \alpha_n^2(t_k) \rangle$, is obtained from the analytical solution of Eq. (10). In this work, the deposition rate is fixed at $W_0=1$ layer/s for all simulations. Eleven substrate temperature values ranging from 300 to 700 K are sampled for the computation of the dependence of the parameters on substrate temperature.

Fig. 6 shows the steady-state values of the expected mean slope square at different substrate temperatures computed from the EW equation with the estimated parameters and from the kMC simulations; the agreement is excellent for all substrate temperatures. The dependence of the model parameters on the substrate temperature is shown in Fig. 7 and is used in the formulation of the model predictive controller. The EW-type equation with parameters estimated under time-invariant operating conditions is suitable for the purpose of model predictive control design because the control input in the MPC formulation is piecewise constant, i.e., the manipulated substrate temperature remains constant between two consecutive sampling times, and thus, the dynamics of the microscopic process can be predicted using the closed-form dynamic models with estimated parameters.

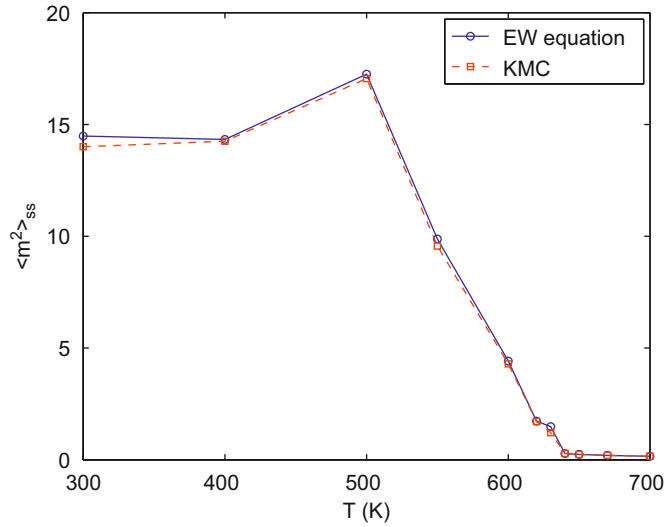


**Fig. 6.** Steady-state values of the expected mean slope square computed from the EW equation (solid line) and from the kMC simulations (dashed line) at different substrate temperatures; $W=1$ layer/s.

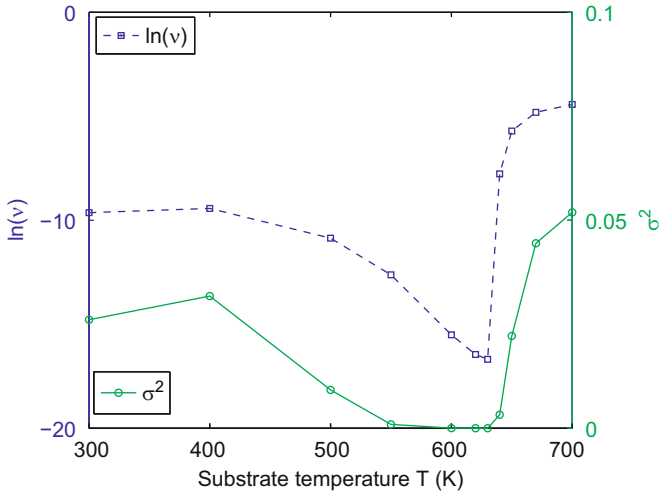


**Fig. 7.** Dependence of $\ln(\nu)$ and $\sigma^2$ on substrate temperature; $W=1$ layer/s.

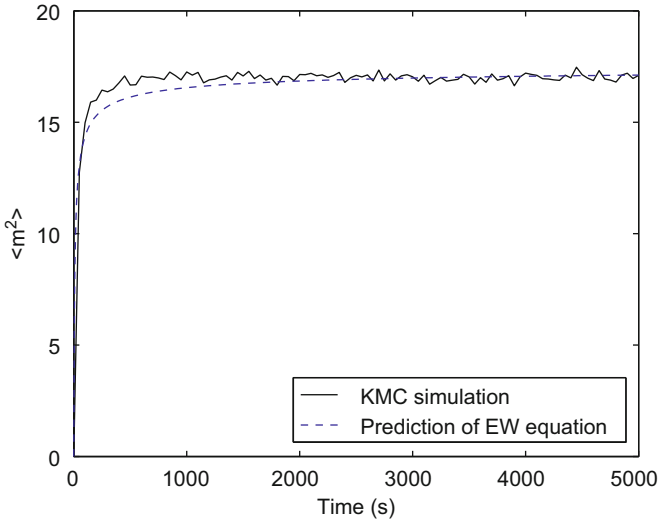


**Fig. 8.** Comparison of EW-model prediction and kMC simulation results for $\langle m^2 \rangle$; $T=500$ K and $W=1$ layer/s.

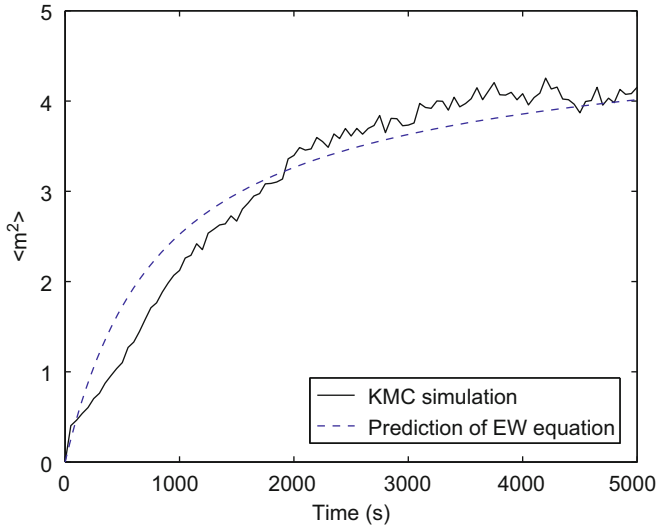


**Fig. 9.** Comparison of EW-model prediction and kMC simulation results for $\langle m^2 \rangle$; $T=600$ K and $W=1$ layer/s.

The temperature dependence of model parameters can be verified by comparing the predictions of the expected mean slope square from the EW equation with the estimated parameters to the corresponding profiles obtained from the KMC simulations, as shown in Figs. 8 and 9. We see that the EW equation with the estimated parameters is consistent with the kMC simulations in terms of the expected mean slope square at varying substrate temperatures.

It has been demonstrated that for a broad range of temperature variation the porous thin film growth process exhibits EW-type behavior (Hu et al., 2009a). Thus, each time a new temperature condition (control actuation) is applied to the thin film growth process, the process follows the EW equation behavior but with different model parameters, which depend on the new temperature condition.

## 4. Model predictive control

In this section, a model predictive controller is developed on the basis of the constructed closed-form dynamic model. The control objective is to regulate the expected mean slope square

and the expected surface roughness square of the thin film to desired levels which optimize the light trapping efficiency, i.e., minimizing or maximizing the light reflectance of the surface or interface in thin-film solar cells. The dynamics of the mean slope square and of the surface roughness square are described by the EW equation of the surface height profile of Eq. (5) with appropriately estimated parameters.

### 4.1. MPC formulation

In this subsection, we consider the problem of regulation of RMS slope and RMS roughness of thin film to desired levels within a model predictive control framework. The expected values of mean slope square and of surface roughness square, $\langle m^2 \rangle$ and $\langle r^2 \rangle$, are chosen as the control objectives. The substrate temperature is used as the manipulated input. When temperature is used as the manipulated input, the deposition rate is fixed at a certain value, $W_0$, during the entire closed-loop simulation. To account for a number of practical considerations, several constraints are added to the controller. First, there is a constraint on the range of variation of the substrate temperature. This constraint ensures validity of the on-lattice kMC model. Another constraint is imposed on the rate of change of the substrate temperature to account for actuator limitations. The control action at time $t$ is obtained by solving a finite-horizon optimal control problem. The cost function in the optimal control problem includes penalty on the deviation of $\langle r^2 \rangle$ and $\langle m^2 \rangle$ from their set-point values, which are computed to optimize the light reflectance of the thin film. The optimization problem is subject to the dynamics of the surface height. The optimal temperature profile is calculated by solving a finite-dimensional optimization problem in a receding horizon fashion. Specifically, the MPC problem is formulated as follows:

$$\min_{T_1,\ldots,T_i,\ldots,T_p} \quad J=\sum_{i=1}^{p}\left\{q_{m^2,i}\left[\frac{m^2_{\mathrm{set}}-\langle m^2(t_i)\rangle}{m^2_{\mathrm{set}}}\right]^2+q_{r^2,i}\left[\frac{r^2_{\mathrm{set}}-\langle r^2(t_i)\rangle}{r^2_{\mathrm{set}}}\right]^2\right\}$$

$$\text{subject to} \quad \frac{\partial h}{\partial t}=r_h+\nu\frac{\partial^2 h}{\partial x^2}+\xi(x,t),$$

$$r^2(t)=\frac{1}{2L_0}\int_{-L_0}^{L_0}[h(x,t)-\bar{h}(t)]^2\,dx,$$

$$m^2(t)=\frac{1}{2L}\sum_{i=1}^{2L}\left(\frac{h_{i+1}-h_i}{\Delta x}\right)^2,$$

$$T_{\min}<T_i<T_{\max}, \quad \left|(T_{i+1}-T_i)/\Delta\right|\le L_T,$$

$$i=1,2,\ldots,p, \tag{16}$$

where $t$ is the current time, $\Delta$ is the length of the sampling interval, $p$ is the number of prediction steps, $p\Delta$ is the specified prediction horizon, $t_i$, $i=1,2,\ldots,p$, is the time of the $i$th prediction step ($t_i=t+i\Delta$), $T_i$, $i=1,2,\ldots,p$, is the substrate temperature at the $i$th step ($T_i=T(t_i)$), $q_{r^2,i}$ and $q_{m^2,i}$, $i=1,2,\ldots,p$, are the weighting penalty factors for the deviations of $\langle r^2 \rangle$ and $\langle m^2 \rangle$ from their respective set-points, $r^2_{\mathrm{set}}$ and $m^2_{\mathrm{set}}$, at the $i$th prediction step, $T_{\min}$ and $T_{\max}$ are the lower and upper bounds on the substrate temperature, respectively, and $L_T$ is the limit on the rate of change of the substrate temperature. The optimal temperature profile, ($T_1$, $T_2$,…,$T_p$), is obtained from the solution of the optimization problem of (16), which minimizes the deviation of the expected mean slope square and of the expected surface roughness square from their respective set-point values within the prediction horizon.

The EW equation model is a stable system, guaranteed by the eigenspectrum of the second-order spatial differential operator with a positive coefficient. In this work, the optimization formulations in the MPC algorithms are solved on an open-loop operating basis at each sampling time (even though feedback is included at each sampling time via the measurements). Thus, the inherent stability of the EW-equation model ensures a stable closed-loop operation under the model predictive controller.

### 4.2. MPC formulation based on finite-dimensional approximations

The surface roughness square and the mean slope square in terms of the state variance, Eqs. (12) and (14), respectively, require computation of infinite sums. Thus, the model predictive controller of (16) is infinite-dimensional and cannot be implemented in practice. To this end, finite-dimensional approximations (with a sufficiently large number of slow modes) can be used to approximately predict the dynamics of the surface roughness square and of the mean slope square as follows:

$$\langle \tilde{r}^2(t)\rangle=\frac{1}{2L_0}\sum_{n=1}^{N}\langle\alpha_n^2(t)\rangle, \quad \langle \tilde{m}^2(t)\rangle=\sum_{n=1}^{N}K_n\langle\alpha_n^2(t)\rangle, \tag{17}$$

where $N$ denotes the dimension of the approximation and the tilde symbols denote the association of these variables with a finite-dimensional system.

Fig. 10 shows the profiles of the reconstructed surface roughness square and mean slope square obtained from the finite-dimensional approximations of Eq. (17) and compares them with the values of the surface roughness square and of the mean slope square computed from the definitions of Eqs. (2) and (3). It can be seen from Fig. 10 that as the order of the approximation increases, the reconstructed values are approaching the actual values computed from the definitions. Thus, the finite-dimensional approximation, that contains a finite number of modes, can be used for model prediction in the model predictive control formulation. Note that, although a higher-order model generally yields a more accurate approximation, the choice of the dimension of the reduced-order model is limited by the lattice size/discretization size. In the closed-loop simulations, the values of states are reconstructed from the discrete surface height profile by taking the inner product with the adjoint eigenfunctions. Due to the finite number of discrete surface height points, there is a limited number (half of the discrete surface height points) of states (modes) that can be used to obtained correct estimates of the surface roughness square and of the mean slope square. This limited availability of the states is an additional reason for using a reduced-order model in the MPC formulation. The MPC

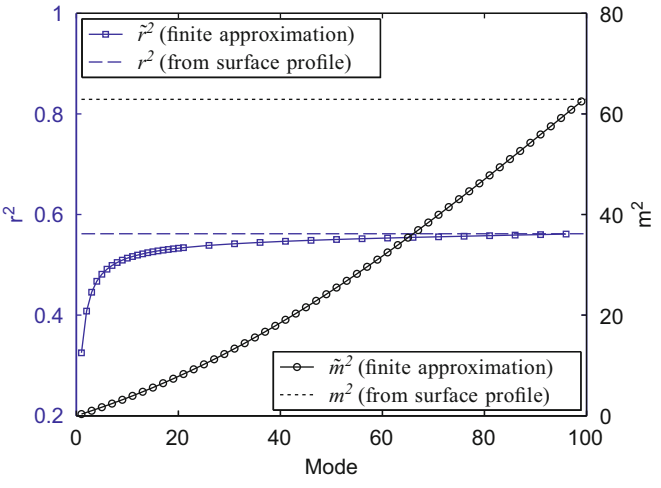


**Fig. 10.** Profiles of reconstructed surface roughness square and mean slope square from the finite-dimensional approximation.

formulation based on the finite-dimensional approximation of the EW equation has the following form:

$$\min_{T_1,\ldots,T_i,\ldots,T_p} \quad J=\sum_{i=1}^{p}\left\{q_{m^2,i}\left[\frac{m^2_{\text{set}}-\langle\tilde{m}^2(t_i)\rangle}{m^2_{\text{set}}}\right]^2+q_{r^2,i}\left[\frac{r^2_{\text{set}}-\langle\tilde{r}^2(t_i)\rangle}{r^2_{\text{set}}}\right]^2\right\}$$

$$\text{subject to} \quad \langle\alpha_n^2(t_i)\rangle=-\frac{\sigma^2}{2\lambda_n}+\left(\alpha_n^2(t)+\frac{\sigma^2}{2\lambda_n}\right)e^{2\lambda_n i\Delta},$$

$$\langle\tilde{r}^2(t_i)\rangle=\frac{1}{2L_0}\sum_{n=1}^{N}\langle\alpha_n^2(t_i)\rangle,$$

$$\langle\tilde{m}^2(t_i)\rangle=\sum_{n=1}^{N}K_n\langle\alpha_n^2(t_i)\rangle,$$

$$T_{\min}<T_i<T_{\max}, \quad |(T_{i+1}-T_i)/\Delta|\le L_T,$$

$$i=1,2,\ldots,p. \tag{18}$$

## 5. Closed-loop simulations

In this section, we apply the proposed predictive controller of (18) to the kMC model of the thin film deposition process to regulate the surface slope and roughness at desired levels. The substrate temperature is used as the manipulated variable, which can be implemented via a heating/cooling system. The adsorption rate is kept constant during all deposition runs. The controlled variables are the expected values of the mean slope square and of the surface roughness square at the end of the deposition process.

In the closed-loop simulations, the surface height profile is obtained from the surface morphology of the thin film from the kMC simulations and is transferred to the controller (state feedback control) at each sampling time. A finite number of slow modes are reconstructed from the surface height profile and are used to calculate the predictions of the mean slope square and of the surface roughness square along the prediction horizon. The estimated parameters and the dependence of the parameters on substrate temperature is used when solving the optimization problem in the model predictive controller. The constrained optimization problem formulated in the MPC of (18) is solved and the optimal input temperature profile is obtained and is applied to the closed-loop system. The optimization problem is solved via a local constrained minimization algorithm with a broad set of initial guesses. The measurement of thin film surface morphology is a challenging issue, especially in real-time. Several techniques have been developed that enable surface height measurements during the operation of a deposition process like atomic force microscopy. The surface information can be also obtained by combining the on-line probing and off-line measurements.

After being computed from the solution of the optimization problem, the optimal manipulated input is applied to the thin film growth process in a sample-and-hold fashion, i.e., the substrate temperature remains constant until the next sampling time. The EW model constructed from the open-loop simulation data can be used in the MPC design since the manipulated input in the closed-loop system changes slowly with respect to the dynamics of the evolution of surface roughness and slope.

### 5.1. Separate regulation of surface slope and roughness

We first consider the control problems of separately regulating surface roughness and slope. Specifically, closed-loop simulations of the slope-only control problem are carried out by assigning the following values to the weighting factors in the MPC formulation of (18): $q_{r^2}=0.0$ and $q_{m^2}=1.0$. Two set-point values, $m^2_{\text{set}}=0.5$ and 5, are considered. The order of finite-dimensional approximation used in the MPC formulation is $N=100$. The deposition rate is fixed at $W=1$ layer/s, which is appropriate from a practical standpoint, and the initial substrate temperature is $T=500$ K. The variation of temperature is from 400 to 700 K. The maximum rate of change of the temperature is $L_T=1$ K/s, which is also appropriate from a practical standpoint. The number of prediction steps is $p=5$ and the prediction step size is $\Delta=5$ s. The sampling time is also 5 s. Since the sampling time equals the prediction step size, only the first value of the manipulated input trajectory, $T_1$, is applied to the deposition process (i.e., kMC model) during the time interval between two successive sampling times, $(t,t+\Delta)$. At the time $t+\Delta$, the surface height profile is sampled and the MPC problem of (16) is solved to obtain the next optimal manipulated input trajectory. The closed-loop simulation duration is 1000 s. All expected values are obtained from 200 independent simulation runs to evaluate the statistics of closed-loop performance.

Figs. 11 and 12 show, respectively, the profiles of the expected mean slope square and of the expected substrate temperature in the closed-loop simulation where the set-point of the mean slope square is 0.5. In Fig. 12, the substrate temperature increases linearly from the initial temperature of 500 K due to the constraint on the rate of change of the temperature. At large times

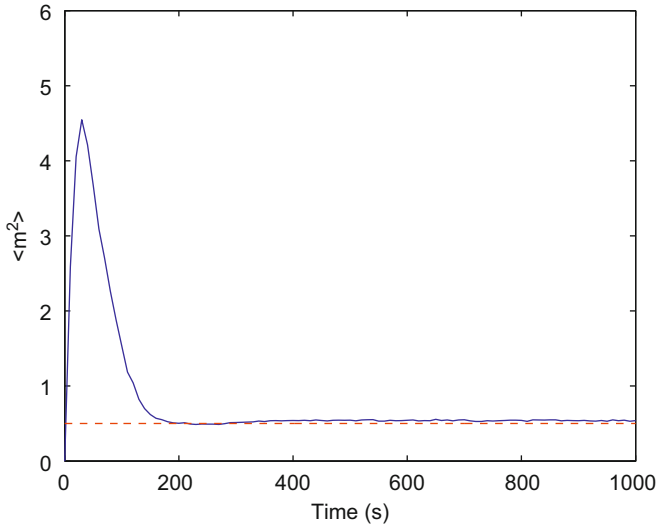


**Fig. 11.** Profile of the expected mean slope square under closed-loop operation (solid line); $m^2_{\text{set}}=0.5$ (dashed line).

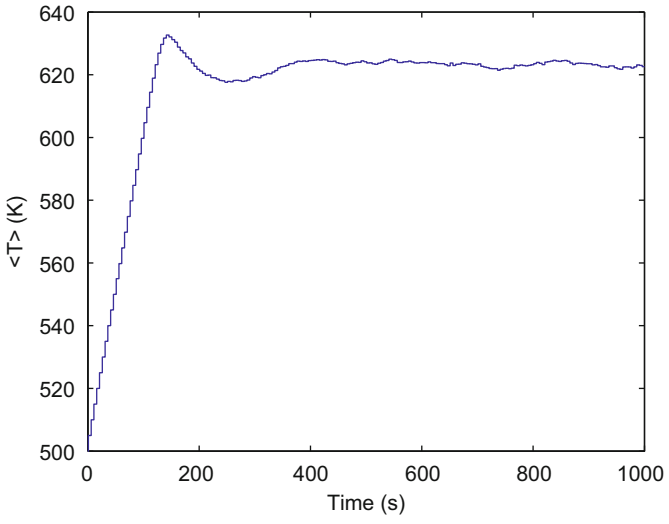


**Fig. 12.** Profile of the expected substrate temperature under closed-loop operation; $m^2_{\text{set}}=0.5$.

($t > 500$ s), the substrate temperature reaches a steady-state value around 620 K. Correspondingly, the expected surface mean slope square initially overshoots and is later regulated at the desired value of 0.5, which can be observed from Fig. 11. The overshoot of the expected mean slope square is the consequence of the constrained increase of the substrate temperature. A less-tight constraint on the rate of change of the substrate temperature or a higher initial substrate temperature may reduce or even avoid this overshoot.

Figs. 13 and 14 show the closed-loop simulation results with a higher set-point value for the mean slope square, $m^2_{set}=5$. The proposed model predictive controller also successfully drives the expected mean slope square to the desired value of 5 within 1000 s.

In addition to the slope-only control problem, the roughness-only control problem is considered with the following weighting factors: $q_{r^2} = 1.0$ and $q_{m^2} = 0.0$. As shown in Fig. 15, the expected surface roughness square is regulated close to the set-point value of 100; a final offset is observed due to the selection of the EW-model parameters that are more sensitive with respect to

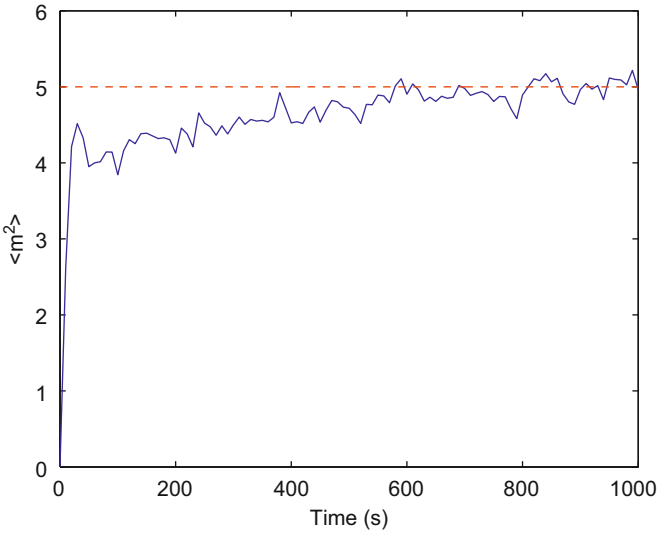


**Fig. 13.** Profile of the expected mean slope square under closed-loop operation (solid line); $m^2_{set}=5$ (dashed line).

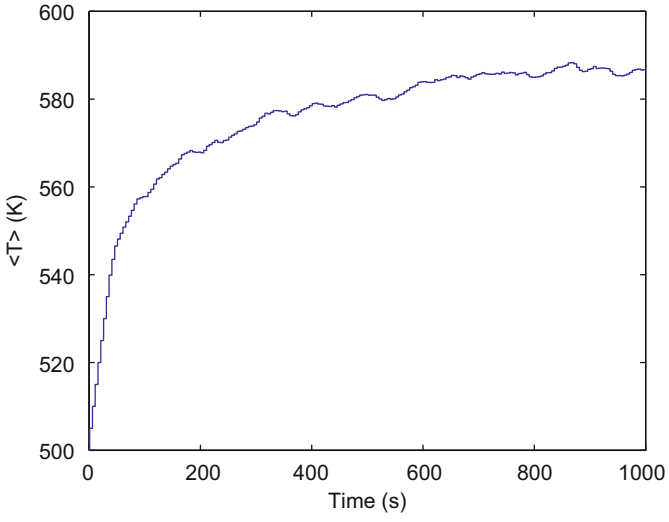


**Fig. 14.** Profile of the expected substrate temperature under closed-loop operation; $m^2_{set}=5$.

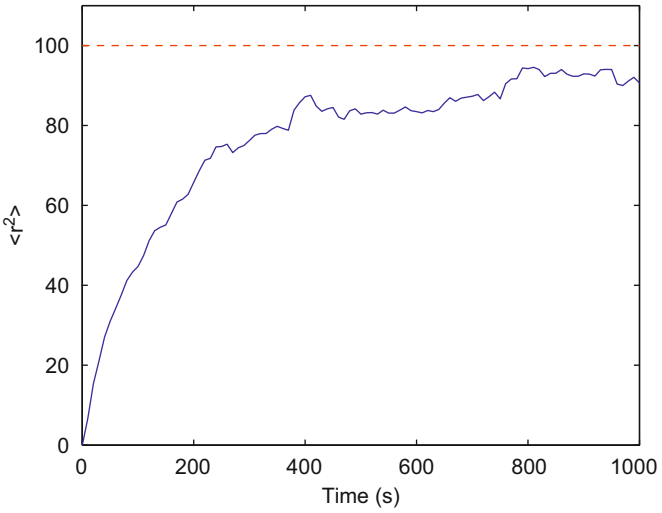


**Fig. 15.** Profile of the expected mean roughness square under closed-loop operation (solid line); $r^2_{set}=100$ (dashed line).

surface slope. This offset can be eliminated if we replace $\langle m^2(t_k)\rangle$ by $\langle r^2(t_k)\rangle$ in the optimization problem of Eq. (15) used for estimating the EW-model parameters. (Specifically, there is a deviation of the expected surface roughness square from the set-point value at the end of the simulation. This deviation is due to fact that the parameter set is estimated solely on the basis of the dynamics of the mean slope square and this parameter set may result in deviations in the prediction of surface roughness square, especially for the intermediate region of the substrate temperature ($500\,\text{K} < T < 650\,\text{K}$). In addition, because there is no penalty on the deviation of RMS slope, $\langle m^2 \rangle$ is far away from its set-point of 0.5 at the end of the roughness-only control closed-loop simulations.)

### 5.2. Simultaneous regulation of surface slope and roughness for light trapping efficiency

Finally, closed-loop simulations of simultaneous regulation of surface slope and roughness are carried out. The set-points of the mean slope square and of the surface roughness square are $m^2_{set}=0.5$ and $r^2_{set}=100$, respectively. Since the substrate temperature is the only manipulated input, the mean slope square and the surface roughness square under closed-loop operations may not reach their respective set-point values. Therefore, a tradeoff between the surface slope and roughness is made by the controller on the basis of the weighting factors of the mean slope square and of the surface roughness square. To simplify the development, the same values of weighting factors of the mean slope square (and the same weighting factors of the surface roughness square) are used for all prediction steps, i.e., $q_{m^2,1} = q_{m^2,2} = \cdots = q_{m^2,5} = = q_{m^2}$ $(q_{r^2,1} = q_{r^2,2} = \cdots = q_{r^2,5} = q_{r^2})$. The weighting factor of mean slope square is kept at 1, while the factor of surface roughness square varies from 1 to 10 000. Fig. 16 shows the final expected values of the mean slope square and of the surface roughness square at the end of the closed-loop simulations ($t=1000$ s) at different ratios of the weighting factors, $\lg(q_{r^2}/q_{m^2})$. It is clear that as the weighting on the surface roughness square increases, i.e., a higher value of $\lg(q_{r^2}/q_{m^2})$, the expected surface roughness square approaches more closely its set-point value of 100, while the expected mean slope square deviates from its set-point value of 0.5.

Since the mean slope square and the surface roughness square cannot reach their respective set-points, Fig. 16 also shows different values of the mean slope square and of the surface

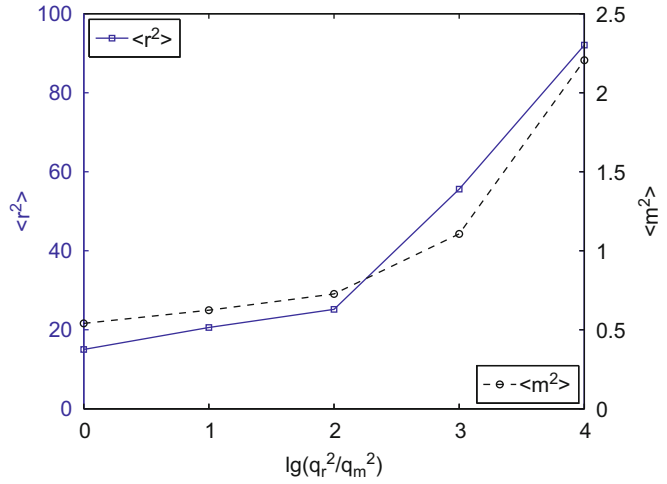


**Fig. 16.** Profiles of $\langle r^2 \rangle$ (solid line) and $\langle m^2 \rangle$ (dashed line) at the end of closed-loop simulations ($t=1000$ s) for different penalty weighting factors: $q_{m^2}=1$ and $1 \le q_{r^2} \le 10\,000$.

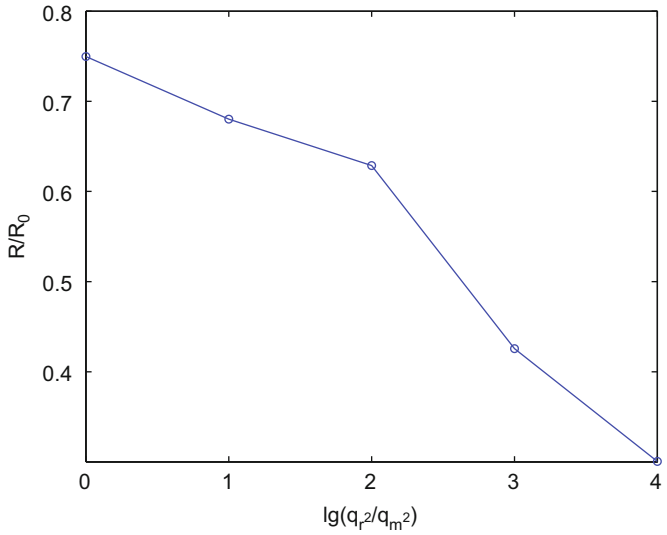


**Fig. 17.** Dependence of light reflectance of thin film on the ratio of the weighting factors, $\lg(q_{r^2}/q_{m^2})$; $r^2_{set}=100$ and $m^2_{set}=0.5$.

roughness square which are obtained at the end of the closed-loop simulations with different weighting factors of the mean slope square and of the surface roughness square. The light reflectance of these thin films obtained from the closed-loop simulations of simultaneous regulation can be computed from the resulting RMS surface slope and RMS roughness using Eq. (1), as shown in Fig. 17. In Fig. 17, the RMS slope, $m$, and the RMS roughness, $r$, are computed as the square roots of $\langle m^2 \rangle$ and $\langle r^2 \rangle$, respectively. The RMS roughness is also scaled with (by multiplying) a physical factor, 6.5 nm, so that the set-point value, $r^2_{set}$, together with $m^2_{set}$, corresponds to an optimal value (maximum) of the light reflectance in Eq. (1).

It can be seen from Fig. 17 that different values of light reflectance of thin film are obtained at different ratios of the weighting factors, $\lg(q_{r^2}/q_{m^2})$. A plot with contours of the light reflectance is given in Fig. 18, which shows the dependence of the RMS slope, the RMS roughness, and the corresponding light reflectance of the thin film on the weighting factors. We note that the values of the RMS roughness in Figs. 17 and 18 are also scaled

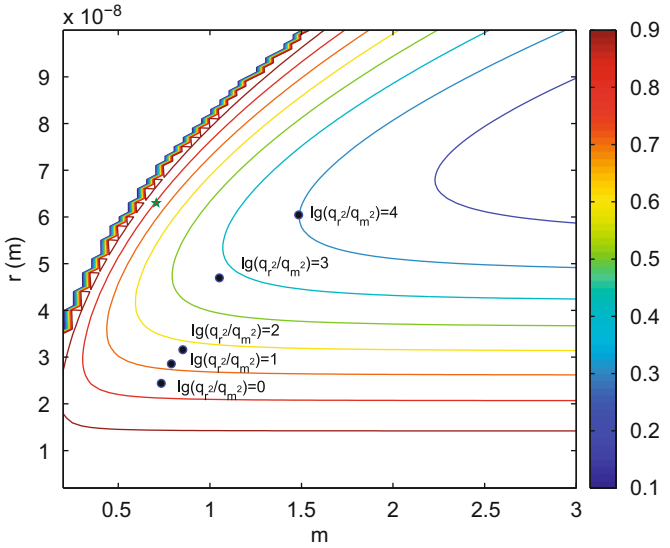


**Fig. 18.** Light reflectance of thin films deposited under closed-loop operations with different weighting schemes.

with the same factor as the one for $r^2_{set}$. An optimal weighting scheme can be determined based on Figs. 17 and 18. For example, in the case where a high light reflectance is desired to improve the light trapping efficiency (e.g., for the back TCO layer that reflects the transmitted light back to the p-i-n layers of the thin film), a combination of the weighting factors, $q_{r^2}=1$ and $q_{m^2}=1$, can be used in the closed-loop operation.

For a perspective of the surface morphology of the thin films, representative snapshots of the film surface microstructure at the end of single open-loop and closed-loop simulations ($t=1000$ s) are shown in Fig. 19. Three closed-loop cases are compared: (1) slope-only control, (2) roughness-only control, and (3) and simultaneous control of slope and roughness. It can bee seen in Fig. 19 that different values of the mean slope square and of the surface roughness square are achieved at the end of simulations. In the open-loop simulation, the substrate temperature and the adsorption rate are fixed and the surface slope and roughness evolve following the open-loop dynamics. In the slope-only and roughness-only control, the mean slope square and the surface roughness square are regulated around their respective set-point values, $m^2_{set}=0.5$ and $r^2_{set}=100$, at the end of the simulation. In the case of simultaneous control of slope and roughness, a trade-off is made between the mean slope square and the surface roughness square. Specifically, different surface height profiles can be observed in Fig. 19 under open-loop operation and under different closed-loop operations. A nearly smooth surface height profile is obtained under slope-only control with a low RMS slope (since the RMS slope set-point, 0.5, is quite low) and a certain level of RMS roughness; these values of RMS slope and roughness result in a reflectance value of $R/R_0=0.69$ which could be appropriate for a back TCO layer. On the other hand, roughness-only control results in a rough surface height profile with both large slope fluctuation (high RMS slope) and large height fluctuation (high RMS roughness); these values of RMS slope and roughness result in a reflectance value of $R/R_0=0.18$ which could be appropriate for a front TCO layer. The surface height profile under simultaneous control of slope and roughness with weighting factor ratio $\lg(q_{r^2}/q_{m^2})=3$ results in an "intermediate" surface height profile, as can be seen in Fig. 19, between slope-only control and roughness-only control, and a reflectance value of $R/R_0=0.46$ which could be appropriate for an intermediate solar cell layer. Therefore, by appropriately choosing the set-points for RMS

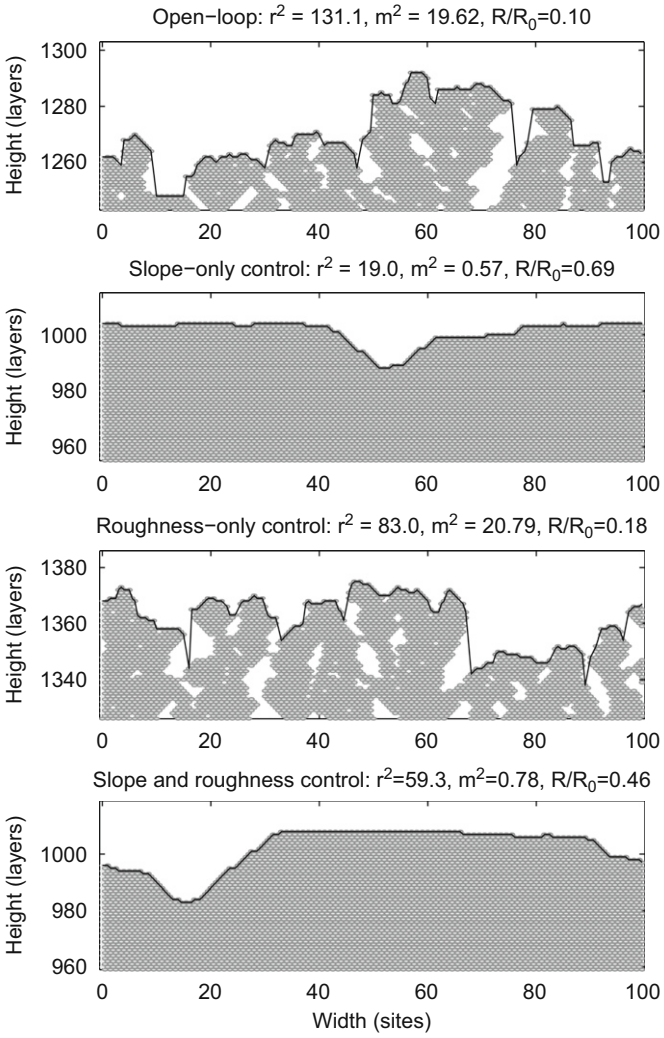


**Fig. 19.** Snapshots of the film microstructure at the end of simulations ($t=1000$ s) under open-loop and closed-loop operations. The open-loop operating conditions: $T = 500$ K and $W=1.0$ layer/s; the set-points in closed-loop simulation: $r^2_{set}=100$ and $m^2_{set}=0.5$; the weighting factor ratio in the simultaneous regulation: $\lg(q_{r^2}/q_{m^2})=3$.

roughness and RMS slope as well as the weighting factors, we can produce layers that have a broad range of reflectance values.

**Remark 3.** In this work, the expected values of roughness and slope are compared to their respective set-points at the end of the deposition ($t=1000$ s). The film thickness is not considered as a control objective. In some applications, there are stringent requirements for specific film thickness. If this is the case, model predictive controllers can be developed for simultaneous regulation of surface roughness, film porosity, and film thickness by including cost penalty on the deviation of film thickness from a desired minimum value or by implementing the thickness requirement as a constraint (Hu et al., 2009c; Zhang et al., in press).

## 6. Conclusions

A model predictive control algorithm was developed to regulate the surface slope and roughness of a thin film growth process. The thin film deposition process was modeled on a one-dimensional triangular lattice that involves two microscopic processes: an adsorption process and a migration process. Kinetic Monte Carlo methods were used to simulate the thin film deposition process. To characterize the surface morphology and to evaluate the light trapping efficiency of the thin film, surface roughness and surface slope were introduced as the root mean squares of the surface height profile and surface slope profile. An EW-type equation was used to describe the dynamics of the surface height profile and predict the evolution of the RMS roughness and RMS slope. A model predictive control algorithm was then developed on the basis of the EW equation model to simultaneously regulate the RMS slope and the RMS roughness at desired levels by optimizing the substrate temperature at each sampling time. The model parameters of the EW equation were estimated from simulation data through least-square methods. Closed-loop simulation results were presented to demonstrate the effectiveness of the proposed model predictive control algorithm in successfully regulating the RMS slope and the RMS roughness at desired levels that optimize thin film light reflectance and transmittance.

## Acknowledgment

Financial support from NSF, CBET-0652131, is gratefully acknowledged.

## References

Bennett, H.E., Porteus, J.O., 1961. Relation between surface roughness and specular reflectance at normal incidence. Journal of the Optical Society of America 51, 123–129.
Christofides, P.D., Armaou, A., Lou, Y., Varshney, A., 2008. Control and Optimization of Multiscale Process Systems. Birkhäuser, Boston.
Davies, H., 1954. The reflection of electromagnetic waves from a rough surface. Proceedings of the Institution of Electrical Engineers 101, 209.
Edwards, S.F., Wilkinson, D.R., 1982. The surface statistics of a granular aggregate. Proceedings of the Royal Society of London Series A—Mathematical Physical and Engineering Sciences 381, 17–31.
Family, F., 1986. Scaling of rough surfaces: effects of surface diffusion. Journal of Physics A: Mathematical and General 19, L441–L446.
Hu, G., Huang, J., Orkoulas, G., Christofides, P.D., 2009a. Investigation of film surface roughness and porosity dependence on lattice size in a porous thin film deposition process. Physical Review E 80, 041122.
Hu, G., Orkoulas, G., Christofides, P.D., 2009b. Modeling and control of film porosity in thin film deposition. Chemical Engineering Science 64, 3668–3682.
Hu, G., Orkoulas, G., Christofides, P.D., 2009c. Regulation of film thickness, surface roughness and porosity in thin film growth using deposition rate. Chemical Engineering Science 64, 3903–3913.
Hu, G., Orkoulas, G., Christofides, P.D., 2009d. Stochastic modeling and simultaneous regulation of surface roughness and porosity in thin film deposition. Industrial & Engineering Chemistry Research 48, 6690–6700.
Huang, J., Hu, G., Orkoulas, G., Christofides, P.D., Dynamics and lattice-size dependence of surface mean slope in thin film deposition. Industrial & Engineering Chemistry Research, in press, doi:10.1021/ie10012w.
Krč, J., Smole, F., Topič, M., 2003. Analysis of light scattering in amorphous Si:H solar cells by a one-dimensional semi-coherent optical model. Progress in Photovoltaics: Research and Applications 11, 15–26.
Krč, J., Zeman, M., 2002. Experimental investigation and modelling of light scattering in a-Si:H solar cells deposited on glass/ZnO:Al substrates. Material Research Society 715, A13.3.1–A13.3.6.
Krč, J., Zeman, M., 2004. Optical modeling of thin-film silicon solar cells deposited on textured substrates. Thin Solid Films 451, 298–302.
Leblanc, F., Perrin, J., 1994. Numerical modeling of the optical properties of hydrogenated amorphous-silicon-based p-i-n solar cells deposited on rough transparent conducting oxide substrates. Journal of Applied Physics 75, 1074.
Levine, S.W., Clancy, P., 2000. A simple model for the growth of polycrystalline Si using the kinetic Monte Carlo simulation. Modelling and Simulation in Materials Science and Engineering 8, 751–762.
Levine, S.W., Engstrom, J.R., Clancy, P., 1998. A kinetic Monte Carlo study of the growth of Si on Si(1 0 0) at varying angles of incident deposition. Surface Science 401, 112–123.
Müller, J., Rech, B., Springer, J., Vanecek, M., 2004. TCO and light trapping in silicon thin film solar cells. Solar Energy 77, 917–930.
Ni, D., Christofides, P.D., 2005. Multivariable predictive control of thin film deposition using a stochastic PDE model. Industrial & Engineering Chemistry Research 44, 2416–2427.

Poruba, A., Fejfar, A., 2000. Optical absorption and light scattering in microcrystalline silicon thin films and solar cells. Journal of Applied Physics 88, 148–160.

Rowlands, S.F., Livingstone, J., Lund, C.P., 2004. Optical modelling of thin film solar cells with textured interfaces using the effective medium approximation. Solar Energy 76, 301–307.

Springer, J., Poruba, A., 2004. Improved three-dimensional optical model for thin-film silicon solar cells. Journal of Applied Physics 96, 5329–5337.

Tao, G., Zeman, M., 1994. Optical modeling of a-Si:H based solar cells on textured substrates. In: 1994 IEEE First World Conference on Photovoltaic Energy Conversion. Conference Record of the 24th IEEE Photovoltaic Specialists Conference-1994 (Cat. no. 94CH3365-4), vol. 1, p. 666.

Varshney, A., Armaou, A., 2005. Multiscale optimization using hybrid PDE/kMC process systems with application to thin film growth. Chemical Engineering Science 60, 6780–6794.

Varshney, A., Armaou, A., 2006. Identification of macroscopic variables for low-order modeling of thin-film growth. Industrial & Engineering Chemistry Research 45, 8290–8298.

Varshney, A., Armaou, A., 2008. Reduced order modeling and dynamic optimization of multiscale pde/kmc process systems. Computers & Chemical Engineering 32, 2136–2143.

Vlachos, D.G., Schmidt, L.D., Aris, R., 1993. Kinetics of faceting of crystals in growth, etching, and equilibrium. Physical Review B 47, 4896–4909.

Wang, L., Clancy, P., 2001. Kinetic Monte Carlo simulation of the growth of polycrystalline Cu films. Surface Science 473, 25–38.

Yang, Y.G., Johnson, R.A., Wadley, H.N.G., 1997. A Monte Carlo simulation of the physical vapor deposition of nickel. Acta Materialia 45, 1455–1468.

Zeman, M., Vanswaaij, R., 2000. Optical modeling of a-Si:H solar cells with rough interfaces: effect of back contact and interface roughness. Journal of Applied Physics 88, 6436–6443.

Zhang, P., Zheng, X., Wu, S., Liu, J., He, D., 2004. Kinetic Monte Carlo simulation of Cu thin film growth. Vacuum 72, 405–410.

Zhang, X., Hu, G., Orkoulas, G., Christofides, P.D., Controller and estimator design for regulation of film thickness, surface roughness and porosity in a multiscale thin film growth process. Industrial & Engineering Chemistry Research, in press, doi:10.1021/ic901396g.